

# Numerical Solutions of Inflating Higher Dimensional Global Defects

Satsuki Shimonon<sup>1</sup> and Takeshi Chiba<sup>2,3</sup>

<sup>1</sup> *Department of Physics, Kyoto University, Kyoto 606-8502, Japan*

<sup>2</sup> *Department of Physics, College of Humanities and Sciences, Nihon University, Tokyo 156-8550, Japan*

<sup>3</sup> *Division of Theoretical Astronomy, National Astronomical Observatory of Japan, Tokyo 181-8588, Japan*

(Dated: August 20, 2018)

We find numerical solutions of Einstein equations and scalar field equation for a global defect in higher dimensional spacetimes ( $\geq 6$ ). We examine in detail the relation among the expansion rate  $H$  and the symmetry-breaking scale  $\eta$  and the number of extra dimensions  $n$  for these solutions. We find that even if the extra dimensions do not have a cigar geometry, the expansion rate  $H$  grows as  $\eta$  increases, which is opposite to what is needed for the recently proposed mechanism for solving the cosmological constant problem. We also find that the expansion rate  $H$  decreases as  $n$  increases.

PACS numbers: 04.50.+h, 98.80.Cq

## I. INTRODUCTION

Recent observations suggest that majority of the Universe is the unknown: 27% is matter (and only 4% is ordinary matter) and the rest is the cosmological constant (or dark energy) [1, 2]. Since the cosmological constant is interpreted as a vacuum energy [3], these observations indicate that the energy density of the vacuum energy is  $\rho_\Lambda \approx (10^{-3}\text{eV})^4$ . On the other hand, a field theoretical estimate of zero point energy of the vacuum yields the Planck energy  $\approx 10^{18}\text{GeV}$ . Therefore, the mismatch between observations and the theory is huge:  $(10^{-3}\text{eV})^4/M_p^4 \simeq 10^{-120}$ . This mismatch is called the cosmological constant problem (CCP) [4, 5] and still remains to be solved.

Dvali *et al.*[6] has suggested the mechanism of diluting the cosmological constant by using brane world models with codimension greater than 2. In this mechanism the observed effective cosmological constant related to the expansion rate becomes small because whose energy is consumed to bend the bulk space even if the bare vacuum energy (brane tension) is as large as the Planck scale. The success of the mechanism rests on the conjectured relation in higher dimension

$$H \simeq M_* \left( \frac{M_*^4}{\rho_{\Lambda 4}} \right)^{1/(n-2)}, \quad (1)$$

where  $M_*$  is the  $(4+n)$ -dimensional Planck mass and  $\rho_{\Lambda 4}$  is the four dimensional (bare) vacuum energy (brane tension). If the number of extra dimensions  $n$  is greater than 2, the expansion rate  $H$  is inversely proportional to the brane tension  $\rho_{\Lambda 4}$ . Then the smallness of the cosmological constant could be explained by the largeness of the brane tension.

Cho and Vilenkin (extending the analytic solutions in [7]) have recently constructed numerical solutions of a global defect in seven ( $n=3$ ) dimensional spacetime [8]. They obtained numerical solutions of an inflating global defect if the symmetric breaking scale is greater than the higher dimensional Planck scale. Then the inflation rate is found to grow almost linearly as the brane tension is

increased, which is opposite to what is needed to solve the cosmological constant problem (1).

The main purpose of this paper is to extend Cho and Vilenkin's model to the arbitrary  $(4+n)$ -dimensional one and find numerical solutions without "cigar ansatz" and to examine the relation among the number of extra-dimensions, the energy density and the expansion rate.

We shall find that the conjectured relation (1) does not hold even by using our new bulk solutions in other extra dimensions  $n(\geq 2)$ . However we find that the brane's expansion rate is a monotonically decreasing function of the number of the extra dimensions  $n$  and can vanish at the specific dimension.

In the following section, we introduce the model in Sec. II. Results of the numerical integration are shown in Sec. III. Finally, we summarize our results in Sec. IV. Some numerical details are given in Appendix A. Cigar type solutions are reexamined in Appendix B.

## II. MODEL

### A. Space-time structure

In our model, the brane is assumed a 4-dimensional de-Sitter space  $\mathbf{dS}^4$ , and the extra space is a spherically symmetric  $n$ -dimensional space  $\mathbf{R} \times \mathbf{S}^{n-1}$ . Where the number of extra dimensions  $n$  is equal to or greater than 2. The entire manifold is wrapped product of both spaces  $\mathbf{R} \times \mathbf{S}^{n-1} \times \mathbf{dS}^4$ , whose metric is

$$ds^2 = dr^2 + C(r)^2 r^2 d\Omega_{n-1}^2 + B(r)^2 \left( -dt^2 + e^{2Ht} \sum_{i=1}^3 dx^i{}^2 \right). \quad (2)$$

Here the coordinate of the brane is  $(t, x^1, x^2, x^3)$  and  $H$  is the positive constant expansion rate. The extra space's coordinate is  $(r, \theta_1, \dots, \theta_{n-1})$  and  $d\Omega_{n-1}$  is the metric of an  $n-1$  dimensional sphere  $\mathbf{S}^{n-1}$ .  $C(r)r$  and  $B(r)$  are the radius of the extra space and the warp factor depending on  $r$  only. We adopt the Einstein-Hilbert action for the

space-time dynamics such that

$$\mathcal{S}_{\text{E-H}} = \frac{1}{2\kappa^2} \int d^{4+n}x \sqrt{-g} \mathcal{R}, \quad (3)$$

where  $\kappa^2 = 1/M_*^{2+n}$  with  $M_*$  being the  $(4+n)$ -dimensional Planck mass.

### B. Energy Momentum Tensor

The global defect in the  $n$ -dimensional spherically symmetric space is introduced to construct the brane, which is described by a multiplet of the scalar fields  $\phi^i$  with the action,

$$\mathcal{S}_\phi = \int d^{4+n}x \sqrt{-g} \left[ -\frac{1}{2} \partial^A \phi^i \partial_A \phi_i - V(\phi) \right], \quad (4)$$

where capital letters ( $A, \dots$ ) and small letters ( $i, \dots$ ) run from 1 to  $4+n$  and from 1 to  $n$  respectively. Because we consider spherically symmetric solutions only, the scalar multiplet has been assumed to have a hedgehog configuration,  $\phi^i = \phi(r)\xi^i/r$ . Here  $\phi(r)$  depends only on the radius coordinate  $r$  and  $\xi^i$  represent for the Cartesian coordinates of the extra space. The potential of the scalar field  $V(\phi)$  has minimum at  $|\phi^i| = \phi = \eta$  such that

$$V(\phi) = \frac{\lambda}{4} (\phi^2 - \eta^2)^2. \quad (5)$$

The energy density due to the scalar field may be regarded as the brane tension.

### C. Basic Equations

The Einstein equations and the equation of motion of the scalar field are derived from the action, Eq.(3) and Eq.(4). The Einstein equations are

$$\begin{aligned} G^\mu{}_\mu &= -\frac{1}{4} \frac{{}^{(4)}R}{B^2} + 3\frac{B''}{B} + 3\left(\frac{B'}{B}\right)^2 \\ &+ 3(n-1)\left(\frac{B'}{Br} + \frac{B'C'}{BC}\right) \\ &+ (n-1)\frac{C''}{C} + \frac{(n-2)(n-1)}{2}\left(\frac{C'}{C}\right)^2 \\ &+ n(n-1)\frac{C'}{Cr} + \frac{(n-2)(n-1)}{2}\left(\frac{1}{r^2} - \frac{1}{C^2r^2}\right) \\ &= \kappa^2 \left[ -\frac{\phi'^2}{2} - \frac{(n-1)\phi^2}{2C^2r^2} - \frac{\lambda}{4}(\phi^2 - \eta^2)^2 \right], \quad (6) \end{aligned}$$

$$\begin{aligned} G^r{}_r &= 6\left(\frac{B'}{B}\right)^2 + 4(n-1)\left(\frac{B'}{Br} + \frac{B'C'}{BC}\right) \\ &+ \frac{(n-2)(n-1)}{2}\left(\frac{C'}{C}\right)^2 + (n-2)(n-1)\frac{C'}{Cr} \\ &+ \frac{(n-2)(n-1)}{2}\left(\frac{1}{r^2} - \frac{1}{C^2r^2}\right) - \frac{1}{2}\frac{{}^{(4)}R}{B^2} \\ &= \kappa^2 \left[ \frac{\phi'^2}{2} - \frac{(n-1)\phi^2}{2C^2r^2} - \frac{\lambda}{4}(\phi^2 - \eta^2)^2 \right], \quad (7) \end{aligned}$$

$$\begin{aligned} G^{\theta_i}{}_{\theta_i} &= -\frac{1}{2}\frac{{}^{(4)}R}{B^2} + 4\frac{B''}{B} + 6\left(\frac{B'}{B}\right)^2 \\ &+ 4(n-2)\left(\frac{B'}{Br} + \frac{B'C'}{BC}\right) + (n-2)\frac{C''}{C} \\ &+ \frac{(n-3)(n-2)}{2}\left(\frac{C'}{C}\right)^2 + (n-1)(n-2)\frac{C'}{Cr} \\ &+ \frac{(n-3)(n-2)}{2}\left(\frac{1}{r^2} - \frac{1}{C^2r^2}\right) \\ &= \kappa^2 \left[ -\frac{\phi'^2}{2} - \frac{(n-3)\phi^2}{2C^2r^2} - \frac{\lambda}{4}(\phi^2 - \eta^2)^2 \right]. \quad (8) \end{aligned}$$

Here  ${}^{(4)}R = 12H^2$  represents for the 4-dimensional Ricci scalar depending on the expansion rate of the brane. The prime denotes the differentiation with respect to  $r$ . The equation of motion of the scalar field is

$$\begin{aligned} \phi'' + (n-1)\left(\frac{4}{(n-1)}\frac{B'}{B} + \frac{C'}{C} + \frac{1}{r}\right)\phi' \\ - (n-1)\frac{\phi}{C^2r^2} - \lambda\phi(\phi^2 - \eta^2) = 0. \quad (9) \end{aligned}$$

Eq.(7) imposes the constraint when solving eq. (6), (8) and (9) as the second-order differential equations for  $B$ ,  $C$  and  $\phi$ .

### III. NUMERICAL SOLUTIONS

We have solved the Eq. (6), (7), (8) and (9) numerically with the initial conditions  $B(0) = C(0) = 1$ ,  $B'(0) = C'(0) = 0$  and  $\phi(0) = 0$ . These equations have a set of three parameters  $(n, \kappa\eta, (\kappa/\lambda^{1/2})H)$ . It is found by the numerical integration that the proper relation among them is obtained under the condition that the point of a singularity becomes as far as possible. We assume that only particular combination of these parameters gives a nondiverging solution. We shall call such parameters eigenvalues and regard regular solutions with eigenvalues as physical solutions. Solutions obtained from parameters deviated from the eigenvalues have divergence in  $B$  or  $C$ . Similar situations are considered in [8] for the cigar ansatz which is detailed in Appendix B. We shall find yet another numerical solutions. The set of eigenvalues forms the surface in the 3-dimensional parameter

space, whose shape also will be studied in the following. The discussion of technical details for finding numerical solutions is given in Appendix A.

### A. Asymptotic Solutions

For  $H = 0$ , we can find an asymptotic solution analytically which is obtained by solving Eq.(6), (7), (8) and (9) at large  $r$ . If  $n \geq 3$ , the solution is

$$\phi(\infty) = \eta, \quad (10)$$

$$B^2(\infty) = \text{constant}, \quad (11)$$

$$C^2(\infty) = 1 - \frac{(\kappa\eta)^2}{n-2}, \quad (12)$$

where  $(\kappa\eta)^2 \leq n-2$ . From Eq. (12), the sphere  $\mathbf{S}^{n-1}$  has a solid angle deficit such that

$$\Delta\Omega = \frac{2\pi^{n/2}}{\Gamma(n/2)} \cdot \frac{(\kappa\eta)^2}{n-2}, \quad (13)$$

where  $\Gamma$  is the gamma function. As  $\kappa\eta$  approaches  $\sqrt{n-2}$ , the deficit angle consumes the entire area. If  $n = 2$ ,  $C(\infty)$  can take an arbitrary constant.

### B. $(\kappa\eta)^2 \leq n-2$ Case

For  $(\kappa\eta)^2 \leq n-2$ , a non-singular solution exists when the brane is not expanding,  $H = 0$ . Then, the solution takes an asymptotic form given in the last subsection.

We have solved the Einstein equations and the equation of motion of  $\phi$  numerically in the range of  $[0, r_{\max}]$ . Here  $r_{\max}$  should be taken to be sufficiently large so that  $\phi$  takes a constant value given in Eq. (10). The details of the method of numerical integration is given in Appendix A.

As an example, Fig. 1 shows a solution with the parameter  $(n, \kappa\eta, (\kappa/\lambda^{1/2})H) = (3, 0.65, 0)$ . The scalar field  $\phi$  approaches  $\eta$  rapidly, which makes the defect core with the energy density  $(\kappa\eta)^4$  approximately, and  $B(r)$  and  $C(r)$  approach toward constants as Eq. (10), (11) and (12).

### C. $(\kappa\eta)^2 > n-2$ Case

For  $(\kappa\eta)^2 > n-2$ , arbitrary  $H$  including  $H = 0$  leads to a divergence in  $B$  or  $C$  at finite distance from the origin and the singularity is formed. We call this point  $r_{\text{sing}}$ . At the specific value of  $H$ , the distance to the singularity becomes as far as possible and the divergence

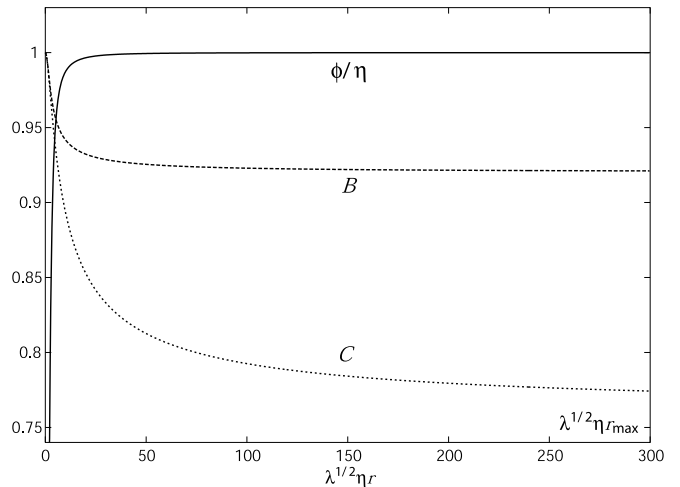


FIG. 1: This graph shows a solution with the eigenvalue  $(n, \kappa\eta, (\kappa/\lambda^{1/2})H) = (3, 0.65, 0)$ .

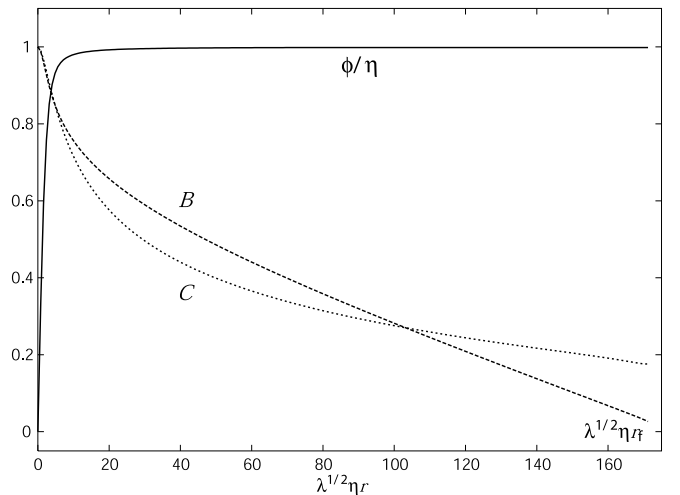


FIG. 2: This graph shows the solution with the eigenvalue  $(n, \kappa\eta, (\kappa/\lambda^{1/2})H) = (3, 1.09, 0.003786056)$ .  $B$  approaches toward 0 at finite  $r_f$ .

vanishes. We call this point  $r_f$ . We note that a fine-tuning of the parameters is required to find this local peak of the distance. The details of the numerical method is given in Appendix A.

As an example, the numerical solution with the eigenvalue  $(n, \kappa\eta, (\kappa/\lambda^{1/2})H) = (3, 1.09, 0.003786056)$  is shown in Fig. 2. It is noticed that the  $B(r)$  vanishes at finite  $r$  but  $C(r)$  does not diverge. The solutions for other dimensions can be obtained and are shown in Fig. 3.

Fig. 4 shows the relations between  $\eta$  and  $H$  with  $n$  fixed at some values. Each line approaches the point  $(\kappa\eta, H) = (\sqrt{n-2}, 0)$ . We find that  $H$  grows as  $\eta$  is increased. This tendency is similar to the Friedmann equation but opposite to the conjectured relation Eq.(1).

Fig. 5 shows the relations between  $n$  and  $H$  with  $\eta$

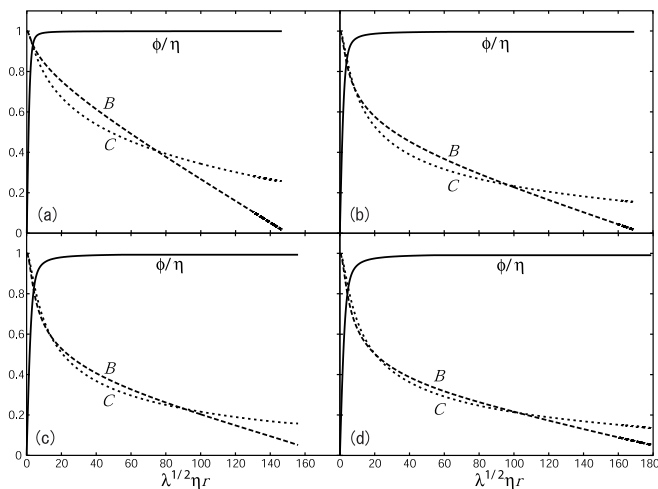


FIG. 3: (a), (b), (c) and (d) are for the eigenvalues  $(n, \kappa\eta, (\kappa/\lambda^{1/2})H) = (2, 0.65, 0.003467)$ ,  $(4, 1.46, 0.004330)$ ,  $(5, 1.765, 0.004535)$  and  $(6, 2.025, 0.004119)$  respectively.

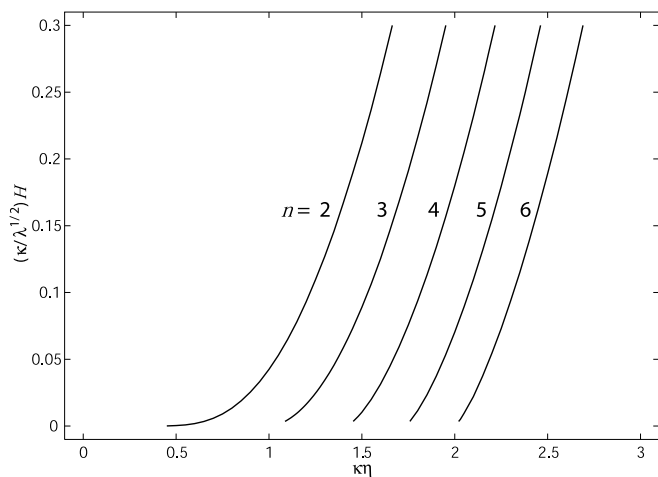


FIG. 4: The relation between  $\eta$  and  $H$  with  $n$  fixed respectively. In the region where  $H$  is small, we cannot find eigenvalue, because the point of singularity is very far from the origin.  $H = 0$  seems to be established at  $\kappa\eta = \sqrt{n-2}$ .

fixed at some values. At  $n = 0$  in this figure, the values read from the usual four-dimensional Friedmann equation,  $H^2 = \kappa^2\rho/3$ ,  $\rho = \lambda\eta^4/4$  are also indicated. This figure shows that the expansion rate determined by the Friedmann equation is suppressed as the number of extra-dimensions increases and  $H$  vanished at a specific dimension. This effect may be considered as the dilution of the cosmological constant. However, very small but non-zero expansion rate of  $H \sim 10^{-33}\text{eV}$  cannot be reproduced without a fine-tuning for  $\kappa\eta$ .

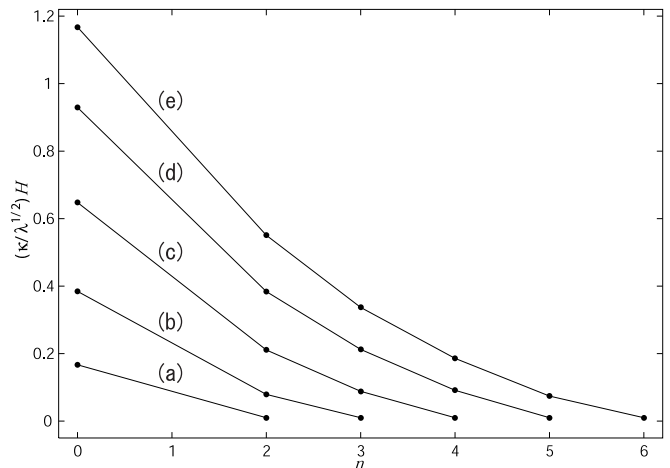


FIG. 5: The relations between  $n$  and  $H$ . (a), (b), (c), (d) and (e) were given by fixing  $\kappa\eta = 0.760, 1.15, 1.50, 1.80, 2.01$  respectively. Values the normal Friedmann equation holds are also indicated at  $n = 0$ . As the number of extra-dimensions increase, the expansion rate is suppressed. The end points of each lines are  $(n, H) = (n, 0.01)$ .

#### IV. CONCLUSION

We have solved the Einstein equations and the scalar field equation for a global defect in higher dimensional spacetimes ( $\geq 6$ ). The defect has a (3+1) dimensional core in  $n \geq 2$  extra dimensions. We have extended the analysis by Cho and Vilenkin [8] to other extra dimensions and found numerical solutions without ‘‘cigar ansatz’’. We have examined in detail the relation among the expansion rate  $H$  and the symmetry-breaking scale  $\eta$  and the number of extra dimensions  $n$  for these solutions. We find that even if the extra dimensions do not have a cigar geometry, the expansion rate  $H$  grows as  $\eta$  increases, which is opposite to what is needed for the recently proposed mechanism [6] for solving the cosmological constant problem. Finally we want to notice that our nondiverging solutions require fine-tuning of parameters  $(n, \kappa\eta, (\kappa/\lambda^{1/2})H)$ . So the problem of fine-tuning remain exist even if  $H$  decreases as  $\eta$  increases.

#### Acknowledgments

It is a pleasure to thank Takashi Nakamura for stimulating discussions throughout the course of this work. We acknowledge our colleagues of the Kyoto University for hospitality. This work was supported in part by a Grant-in-Aid for Scientific Research (No.15740152) from the Japan Society for the Promotion of Science, and also supported by a Grant-in-Aid for the 21st Century COE ‘‘Center for Diversity and Universality in Physics’’.

## APPENDIX A: NUMERICS

In this Appendix, we give the details for finding the numerical solutions.

### 1. $(\kappa\eta)^2 \leq n - 2$ Case

In this case, our strategy for the calculation is divided into 2 steps.

1. Firstly numerically integrating Eq. (6), (8) and (9) as an initial value problem from the origin.
2. Then solving them as a two-point value problem by the relaxation method with the initial solutions obtained by the previous step.

In the Step 1, we solve the differential equations by the 4th-order Runge-Kutta method. The calculation starts from the origin with the initial conditions,  $B(0) = C(0) = 1$ ,  $B'(0) = C'(0) = 0$ ,  $\phi(0) = 0$  and different  $\phi'(0)$ . The calculation is so sensitive to the initial condition,  $\phi'(0)$ , that bad choice would lead to the divergence of  $B, C, \phi$  at finite distance. So we have fine tuned the sixth initial condition  $\phi'(0)$  so that the point of divergence goes as far away as possible which we call  $r_{\text{lim}}$ . Then we can obtain an approximate solution in the range  $[r_{\text{lim}}, r_{\text{max}}]$  without numerical divergence by fixing  $\phi(r) = \phi(r_{\text{lim}})$  at  $r \geq r_{\text{lim}}$  artificially. In the Step 2, we solve the differential equations by the relaxation method with two point boundary conditions at  $r = 0$  and at  $r_{\text{max}}$ . The sixth condition is now replaced with  $\phi'(r_{\text{max}}) = 0$ . After the iteration converges (typically relative error below  $5 \times 10^{-10}$ ), we finally obtain a solution.

### 2. $(\kappa\eta)^2 > n - 2$ Case

For  $(\kappa\eta)^2 > n - 2$ , arbitrary  $H$  including  $H = 0$  leads to a divergence in  $B$  or  $C$  at finite distance from the origin and the singularity is formed. We call this point  $r_{\text{sing}}$ . At the specific value of  $H$ , the distance to the singularity becomes as far as possible and the divergence vanishes. We call this point  $r_f$ .

We solve the Einstein equations and the equation of motion of  $\phi$  numerically in the range of  $[0, r_{\text{sing}}]$ . But the value of  $r_{\text{sing}}$  remains unknown to be decided by solving accurately. So, our strategy of the calculation is divided into 4 steps.

1. Firstly numerically integrating Eq. (6), (8) and (9) as an initial value problem from the origin.
2. Then solving them as a two-point value problem by the relaxation method with the initial solutions obtained by the previous step.
3. Extending the solution of  $\phi$  to sufficiently large value of  $r$ .

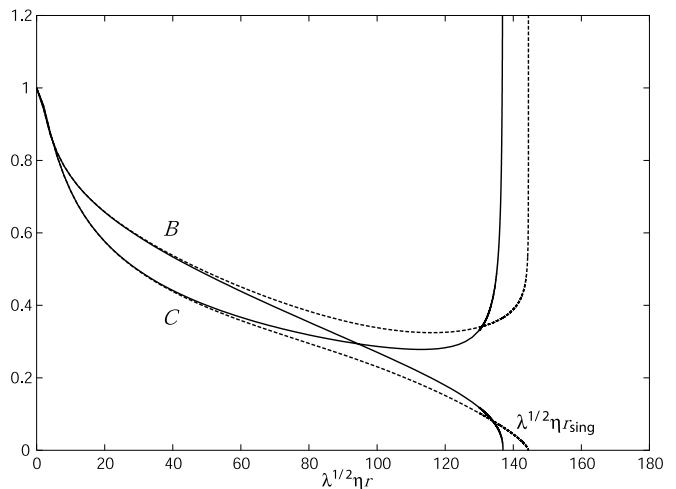


FIG. 6: This graphs shows solutions which have singularity. The solid line and the broken line is for the parameter  $(n, \kappa\eta, (\kappa/\lambda^{1/2})H) = (3, 1.09, 0.00375), (3, 1.09, 0.00400)$ , respectively. These solutions have singularity at finite  $r$ .

4. Numerically integrating the equations with the fixed  $\phi$  obtained in the Step 3 to find the true position of the singularity and the solution.

Step 1 is executed in the same way as Step 1 of  $(\kappa\eta)^2 \leq n - 2$  case. But the range of  $r$  is  $[0, \bar{r}_{\text{sing}}]$ , where the bar means that this position of the singularity is different from the true one. Step 2 is also executed in the same way as  $(\kappa\eta)^2 \leq n - 2$  case. But the boundary condition is imposed at  $r = 0$  and at  $r = \bar{r}_{\text{sing}} - \Delta r$ . The right point is shifted to left by  $\Delta r$  so that the singularity is not included in this range  $[0, \bar{r}_{\text{sing}} - \Delta r]$ . By executing the Step 2, solutions of  $B, C, \phi$  can be obtained and  $\phi'(\bar{r}_{\text{sing}} - \Delta r)$  is vanishing. So we can extend  $\phi(r)$  to sufficiently large value of  $r$ , this procedure is the Step 3. In the Step 4, we solve the differential equations by treating the  $B(r)$  and  $C(r)$  as unknown functions and  $\phi(r)$  as fixed background obtained in Step 3. The algorithm used is the same as Step 1. From the Step 1 to 4, we finally obtain the numerical solutions and the point of the singularity.

Next, we find the "eigenvalue" under the condition that the position of the singularity becomes as far as possible. We can find the unique  $H$  as the eigenvalue with  $(n, \kappa\eta)$  fixed like as follows. If  $H$  is smaller than the eigenvalue, the energy of the defect core bends and closes the bulk space such that  $B(r) \rightarrow 0$  as  $r \rightarrow r_{\text{sing}}$ , which is shown as solid lines in Fig. 6. Then  $C(r)$  diverge at the same point and forming the singularity. As  $H$  is increased, the energy density of the defect is consumed to inflate the brane and the bulk's curvature is relaxed. If  $H$  is beyond the specific value, then that  $B(r) \rightarrow \infty$  at finite distance  $r_{\text{sing}}$ , which is shown as broken lines in Fig. 6. At a very specific value of  $H$  which exists between these two values, neither  $B(r)$  nor  $C(r)$  diverges and the position of the singularity has a local peak here. This  $H$  is to be called the "eigenvalue". Typical examples are

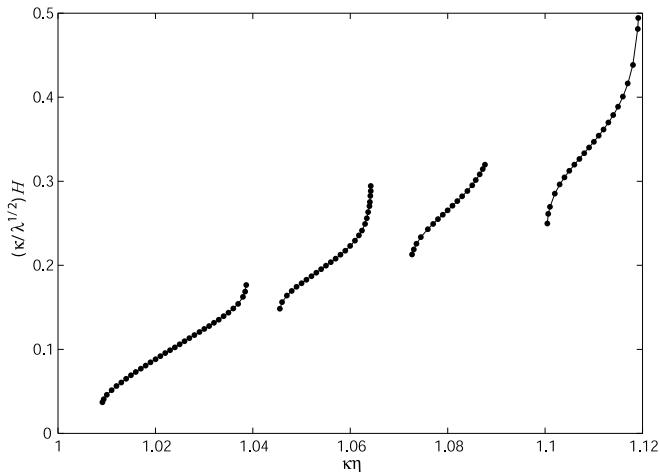


FIG. 7: The relation between  $\eta$  and  $H$  for cigar type solutions with  $n = 3$ .

given in Fig. 2 and Fig. 3.

## APPENDIX B: CIGAR TYPE SOLUTIONS

In the previous works [8, 9], the cigar type solutions in  $n = 3$  case are studied. These solutions have asymptotic forms  $\sqrt{\lambda}\eta Cr \rightarrow \text{constant}$ . The analytic solution for arbitrary  $n \geq 3$  is

$$\kappa^2 \phi^2(r_{\max}) = \frac{2(n^2 - 4) - (n - 1)(\kappa\eta)^2}{(n + 5)}, \quad (\text{B1})$$

$$B(r_{\max}) = \frac{H}{\sqrt{\lambda\eta k}} \sin(\sqrt{\lambda\eta k} r_{\max}), \quad (\text{B2})$$

$$\lambda\eta^2 C^2(r_{\max}) r_{\max}^2 = \frac{(n - 1)(n + 5)(\kappa\eta)^2}{2(n + 2)[(\kappa\eta)^2 - (n - 2)]}, \quad (\text{B3})$$

where

$$k = \sqrt{\frac{n + 2}{2(n + 5)^2} \frac{(\kappa\eta)^2 - (n - 2)}{\kappa\eta}} \quad (\text{B4})$$

and  $r_{\max}$  is a sufficiently large value.

It is concluded in [8] that eigenvalues in  $(\kappa\eta, (\kappa/\lambda^{1/2})H)$  space can be line fitted. But we have reexamined this calculation and found more complex structure shown in Fig. 7.

Our method of the numerical integration is as follows. We have set the seven boundary conditions  $B(0) = C(0) = 1$ ,  $B'(0) = C'(0) = 0$ ,  $\phi(0) = 0$ ,  $\phi'(r_{\max}) = 0$ ,  $(r_{\max}C(r_{\max}))' = 0$ , and considered the equations (6),(8), (9) and  $H'(r) = 0$ , in which  $H$  is treated as the dependent variable of  $r$ . The strategy to solve these equations is the same as described in Appendix A. The iteration is not converged for some values of  $\kappa\eta$  corresponding to the blanks in Fig. 7.

- 
- [1] C. L. Bennett *et al.*, *Astrophys. J. Suppl.* **148**, 1 (2003) [arXiv:astro-ph/0302207]; D. N. Spergel *et al.* [WMAP Collaboration] *Astrophys. J. Suppl.* **148**, 175 (2003) [arXiv:astro-ph/0302209].
  - [2] R. A. Knop *et al.*, *Astrophys. J.* **598**, 102 (2003) [arXiv:astro-ph/0309368]; A. G. Riess *et al.* [Supernova Search Team Collaboration], *Astrophys. J.* **607**, 665 (2004) [arXiv:astro-ph/0402512].
  - [3] Ya.B. Zel'dovich, *Sov. Phys. Usp.* **11**, 381 (1968).
  - [4] S. Weinberg, *Rev. Mod. Phys.* **61**, 1 (1989)
  - [5] P. J. E. Peebles and B. Ratra, *Rev. Mod. Phys.* **75**, 559 (2003).
  - [6] G. Dvali, G. Gabadadze and M. Shifman, *Phys. Rev.* **D67**, 044020 (2003).
  - [7] I. Olasagasti and A. Vilenkin, *Phys. Rev.* **D62**, 044014 (2000).
  - [8] I. Cho and A. Vilenkin, *Phys. Rev.* **D68**, 025013 (2003).
  - [9] I. Cho and A. Vilenkin, *Phys. Rev.* **D69**, 045005 (2004).